

On the disc reflection spectroscopy of NS LMXB Serpens X-1: analysis of a recent *NuSTAR* observation

Aditya S. Mondal^{1*}, G. C. Dewangan², B. Raychaudhuri¹

¹Department of physics, Visva-Bharati, Santiniketan, West Bengal-731235, India

²Inter-University Centre for Astronomy & Astrophysics (IUCAA), Pune, 411007 India

23 July 2019

ABSTRACT

We present *NuSTAR* observation of the atoll type neutron star (NS) low-mass X-ray binary (LMXB) Serpens X-1 (Ser X-1) performed on 17 February 2018. We observed Ser X-1 in a soft X-ray spectral state with 3 – 79 keV luminosity of $L_X \sim 0.4 \times 10^{38}$ erg s⁻¹ ($\sim 23\%$ of the Eddington luminosity), assuming a distance of 7.7 kpc. A positive correlation between intensity and hardness ratio suggests that the source was in the banana branch during this observation. The broadband 3 – 30 keV *NuSTAR* energy spectrum can be well described by a three-component continuum model consisting of a disk blackbody, a single temperature blackbody and a power-law. A broad iron line ~ 5 –8 keV and the Compton back-scattering hump peaking at ~ 10 –20 keV band are clearly detected in the X-ray spectrum. These features are best interpreted by a self-consistent relativistic reflection model. Fits with relativistically blurred disc reflection model suggests that the inner disc R_{in} is truncated prior to the ISCO at $(1.7 - 2.3) R_{ISCO}$ ($\simeq 10.2 - 13.8 R_g$ or 23 – 31 km) and the accretion disc is viewed at an low inclination of $i \simeq 18^\circ - 21^\circ$. The disc is likely to be truncated either by a boundary layer or by the magnetosphere. Based on the measured flux and the mass accretion rate, the maximum radial extension for the boundary layer is estimated to be $\sim 6.4 R_g$ from the NS surface. The truncated inner disc in association with pressure from a magnetic field sets an upper limit of $B \leq 1.6 \times 10^9$ G.

Key words: accretion, accretion discs - stars: neutron - X-rays: binaries - stars: individual Ser X-1

1 INTRODUCTION

A Neutron Star Low Mass X-ray Binary (NS LMXB) is a compact system composed of an NS and a low-mass ($\leq 1 M_\odot$) companion star. NS LMXBs are classified into two main groups based on their X-ray luminosity along with the spectral and the timing properties in X-rays (Hasinger & van der Klis 1989). Those are the so-called “Z” sources, with luminosities close to or above the Eddington luminosity (L_{Edd}) and the “atoll” sources, with luminosities up to $\sim 0.5 L_{\text{Edd}}$ (Homan et al. 2010). The names of the Z and the atoll sources are related to the shape traced in the color-color diagram (CD). The Z sources show three-branches (the horizontal, the normal and the flaring branches) whereas the atoll sources show two main regions in the CD, the island state and isolated from it, the so-called banana branch. The X-ray spectra of the Z sources are soft in all branches and those of the atoll sources are soft at high luminosities and hard at low luminosities.

The harder one is related to the island state and the softer one is related to the banana state which can be further divided as lower banana and upper banana states. However, the relation between the atoll and the Z-track sources is not well understood. Our understanding has improved with the discovery of the source XTE J1701-462 (Remillard et al. 2006) which shows all the characteristics of a Z source as well as an atoll source during its decaying phase (Homan et al. 2010). This implies that whether an NS is an atoll or a Z type is completely determined by the mass accretion rate (Lin et al. 2007).

In NS LMXBs, a geometrically thin, optically thick accretion disc is formed around the NS when it accretes matter from the companion star (Shakura & Sunyaev 1973). The radiation from an accretion disc generates a quasi-thermal spectrum. The accretion discs are usually accompanied by a hot corona (Shakura & Sunyaev 1973) and the coronal emission of such source generates a power-law spectrum by inverse Compton scattering of the thermal disc photon. It is well known that the spectrum from an

* E-mail: adityas.mondal@visva-bharati.ac.in

accretion disc is a multicolor blackbody. At the same time, another hot single-temperature blackbody may potentially arise due to the emission from the boundary layer between the inner accretion disc and the NS surface. This hard X-ray emission (either a power-law continuum or a blackbody component) can irradiate the accretion disc to produce a reflection spectrum. High energy photons tend to Compton scatter back out of the disc, resulting in a broad hump-like shape in the reflection spectrum (Ballantyne et al. 2001; Ross & Fabian 2007). In addition, several narrow emission lines are produced among which Fe K α fluorescent line is the most prominent one because of its high fluorescent yield and large cosmic abundance (Bhattacharyya & Strohmayer 2007; Cackett et al. 2008; Pandel et al. 2008; Reis et al. 2009; Degenaar et al. 2015). The intrinsically narrow Fe K α lines when appear in the X-ray spectra of LMXBs show a broad, asymmetric profile due to Doppler and gravitational shift (Fabian et al. 2000). Studies of Fe K α line profile provide an independent view of the inner accretion flow in NS LMXBs which led to constraints to the inner disc structure and inclination. The accretion disc in NS systems could be truncated by the boundary layer between the disc and the NS surface or by a strong stellar magnetic field. Thus the inner disc radius sets an upper limit to the radius of the NS and hence can constrain the NS equation of state (Piraino et al. 2000; Cackett et al. 2008; Bhattacharyya 2011). Fe K line profile can also be used to obtain an upper limit on the strength of the magnetic field associated with the NS (Ludlam et al. 2019; Degenaar et al. 2016a; King et al. 2016).

The bright persistent atoll type NS LMXB Ser X-1 was discovered in 1965 (Bowyer et al. 1965). Type-1 thermonuclear X-ray bursts have been detected from the source in 1976 (Swank et al. 1976; Li et al. 1977) and it confirms that the compact object in this source is an NS. A super-burst with a duration of approximately 4-hours has also been reported (Cornelisse et al. 2002). The source is located at a distance of 7.7 ± 0.9 kpc (Galloway et al. 2008). The counterpart of Ser X-1 was identified with a main-sequence K-dwarf star (Cornelisse et al. 2013). After its discovery, it has been observed with all major X-ray missions like *ASCA* (Church & Balucińska-Church 2001), *BeppoSAX* (Oosterbroek et al. 2001), *RXTE* (Oosterbroek et al. 2001), *XMM-Newton* (Bhattacharyya & Strohmayer 2007), *Suzaku* (Cackett et al. 2010; Chiang et al. 2016b), *Chandra* (Chiang et al. 2016a) and *NuSTAR* (Miller et al. 2013; Matranga et al. 2017). Several continuum models were used in the previous works, using different combinations of disc blackbody, single temperature blackbody and power-law. Broadband observations preferred a continuum model consisting of all three components (Cackett et al. 2008, 2010; Miller et al. 2013; Chiang et al. 2016b). On the contrary, observations with limited energy ranges preferred two component continuum models, either a disc blackbody and a single temperature blackbody or a single temperature blackbody and a power-law (Bhattacharyya & Strohmayer 2007; Chiang et al. 2016a). Relativistic broad iron lines have been reported from almost all the previous observations (Bhattacharyya & Strohmayer 2007; Cackett et al. 2010; Miller et al. 2013; Chiang et al. 2016b). Different self-consistent reflection models have been used to fit

the reflection component. Spectral differences in different observations may be justified by intrinsic spectral variations of the source (Matranga et al. 2017). Optical spectroscopy and some other X-ray reflection studies indicate towards a low binary inclination $\sim 10^\circ$ (Miller et al. 2013; Cornelisse et al. 2013), although some studies reported the inclination angle in between $25^\circ - 50^\circ$ (Chiang et al. 2016a; Matranga et al. 2017; Cackett et al. 2010). Ser X-1 gives us an opportunity to detect multiple reflection features because of the low-amount of absorbing material in the line of sight of Ser X-1 (corresponding to low neutral hydrogen column density $N_H = 4.0 \times 10^{21} \text{ cm}^{-2}$ Dickey & Lockman 1990).

In the present work, we analyze the latest ~ 31 ks pile-up free *NuSTAR* observation of Ser X-1 in order to give a reliable estimate of the parameters of the system. This observation also allows us to study the source broadband spectrum and to constrain the reflection component such as the broad Fe emission line along with the Compton hump. In this *NuSTAR* observation, the source was captured with a lower luminosity compared to the previous *NuSTAR* observation performed in 2013 (~ 2 times more luminous than the present observation). So, this observation can be useful to test any possible disc truncation scenario at lower luminosity or lower Eddington fraction. This paper is organized in the following manner. First, we describe the observations and the details of data reduction in sec .2. In sec. 3 and sec. 4, we describe the temporal and spectral analysis, respectively. Finally, in sec.5, we discuss our findings.

2 OBSERVATION AND DATA REDUCTION

After observing twice on 2013 July 12 and 13, *NuSTAR* observed the source Ser X-1 again on 2018 February 17 for a total exposure time of ~ 31 ks (Obs. ID: 30363001002). Previous two observations have been analyzed by Miller et al. (2013) and Matranga et al. (2017). *NuSTAR* data of the source Ser X-1 were collected with the two co-aligned grazing incidence hard X-ray imaging Focal Plane Module telescopes (FPMA and FPMB) in the 3 – 79 keV energy band.

We reprocessed the data with the standard *NuSTAR* data analysis software (*NuSTARDAS* v1.7.1) and *CALDB* (v20181030). Using the *nupipeline* tool (version v 0.4.6), we filtered the event lists. We used a circular extraction region with a radius of 100 arcsec centered around the source position to produce a source spectrum for both the telescopes, the FPMA and the FPMB. We used another 100 arcsec circular region away from the source position for the purpose of background subtraction. We created lightcurve, spectra and response files for the FPMA and the FPMB using the *nuproducts* tool. We grouped the FPMA and the FPMB spectral data with a minimum of 500 counts per bin (as the source is relatively bright) and fitted the two spectra simultaneously.

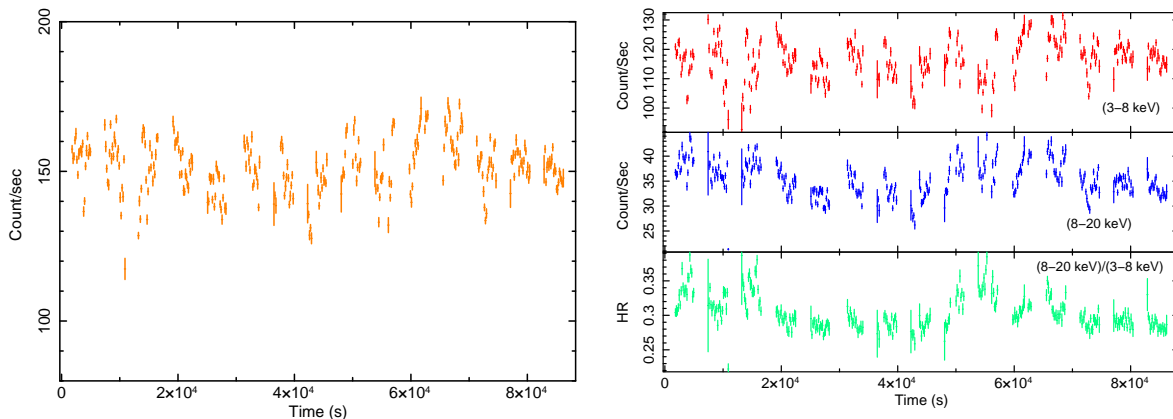


Figure 1. Left: 3–79 keV *NuSTAR*/FPMA light curve of Ser X-1 with a binning of 100 sec. Right: The source count rate in the energy band 3–8 keV and 8–20 keV are shown in the upper and the middle panels, respectively. Bottom panel shows the HR which is the ratio of count rate in the energy band 8–20 keV and 3–8 keV.

3 TEMPORAL ANALYSIS

Left panel of Figure 1 shows the 3–79 keV *NuSTAR*/FPMA light curve of Ser X-1 with a binning of 100 sec and spans ~ 31 ks. Ser X-1 is a bright X-ray source and in this observation it was detected at an average intensity of $\simeq 150$ counts s^{-1} . Ser X-1 is also known for the bursting behaviour but no X-ray bursts were observed during this observation. We also extracted the light curves in the 3–8 keV and 8–20 keV energy ranges, with a bin size of 100 s and presented those separately in the right panel of Figure 1. We generated the hardness ratio (HR) between the photon counts in the above mentioned energy bands and displayed it in the right panel of Figure 1. The HR value, which is a broad measure of the spectral shape, remained fairly constant with a mean value of ~ 0.3 . Although a small count rate variability is observed in the 3–8 keV and 8–20 keV energy band, it is not associated with any significant change in the HR. It suggests that the spectral shape of the source remain stable during the whole span of this particular observation. Additionally, we generated the hardness-intensity diagram (HID), in which the HR (3–8 keV and 8–20 keV photon count ratio) is plotted as a function of the source intensity (3–20 keV), shown in Figure 2. In this observation, the HID shows that the HR is positively correlated with intensity for this source. In the case of atoll sources, the positive correlation between the hardness and the intensity is characteristic to the banana branch (Asai et al. 1993; Hasinger & van der Klis 1989). This means that the source remained in the banana branch rather than in the island branch or in any other period of extreme or unusual behaviour during this observation. Previous *NuSTAR* observation was also found to sample the usual banana branch (Miller et al. 2013). However, it may be noted that the island state has so far not been observed from Ser X-1.

4 SPECTRAL ANALYSIS

We fitted both the *NuSTAR* FPMA and FPMB spectra simultaneously as initial fits revealed a good agreement between these two spectra. An initial inspection of the FPMA and the FPMB spectra also suggests that the source is de-

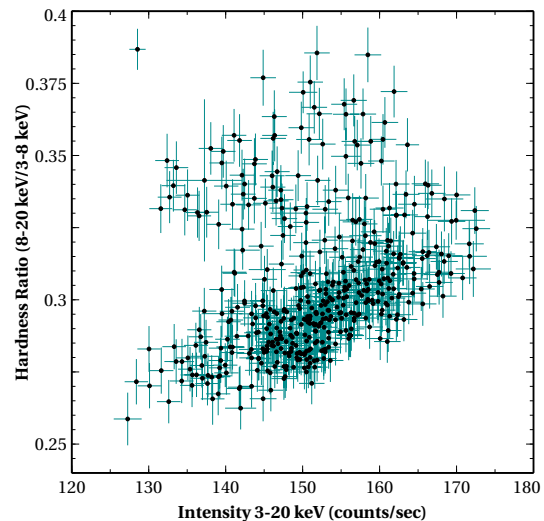


Figure 2. The hardness-intensity diagram (HID) of Ser X-1. Intensity is taken as 3–20 keV source photon count rate and hardness ratio has been taken as the ratio of photon count rate in the energy band 8–20 keV and 3–8 keV. A positive correlation is observed between intensity and the hardness ratio.

tected significantly upto 30 keV. We therefore performed the spectral analysis over the 3–30 keV energy band using XSPEC v 12.9. We added a constant between the spectra to account for uncertainties in the flux calibration of the detectors. The constant was set 1 for the FPMA and left it free for the FPMB. A value of 1.02 was measured for the FPMB. We modelled the interstellar absorption along the line of sight using the *tbabs* model with *vern* cross sections (Verner et al. 1996) and *wilm* abundances (Wilms et al. 2000). For each fit, we fixed the absorption column density to the Dickey & Lockman (1990) value of $4.0 \times 10^{21} \text{ cm}^{-2}$ as the *NuSTAR* data only extends down to 3 keV and found it difficult to constrain from the spectral fits. All the uncertainties in this paper are quoted at 90% of the confidence level if not stated otherwise in particular.

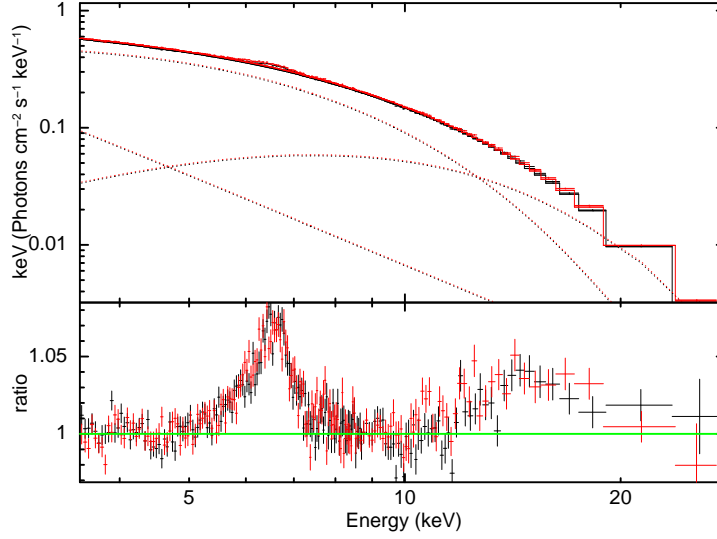


Figure 3. *NuSTAR* (FPMA in black, FPMB in red) unfolded spectra. The data were fit with the model consisting of an absorbed multicolour disk blackbody, a single temperature blackbody and a powerlaw. Model used: `TBabs × (diskbb+bbbody+powerlaw)`. It revealed un-modelled broad emission line $\sim 5 - 8$ keV and a clear hump like feature $\sim 10 - 20$ keV. The prominent residuals can be identified as a broad Fe-K emission line and the corresponding Compton back-scattering hump. The spectral data were rebinned for visual clarity

4.1 Continuum modeling

We fitted 3 – 30 keV *NuSTAR* continuum to a model consisting of a disk blackbody component (`diskbb` in `XSPEC`), a single-temperature blackbody component (`bbbody` in `XSPEC`) and a power-law component (`powerlaw` in `XSPEC`). This combination of models can be interpreted in terms of the emission from the accretion disc, the emission likely caused by the boundary layer/NS surface and the non-thermal emission that may arise through the Comptonization of the soft photons from a hot corona. This combination of models describes the shape of the continuum very well ($\chi^2/dof=2450/739$), but it is not a formally acceptable fit because of the presence of the strong disc reflection features in the spectrum which is evident in Figure 3. We note that, if we eliminate the `powerlaw` component from this continuum model, we get a worse fit, corresponding to a decrease of $\Delta\chi^2 = 191$ for the addition of two parameters when the `powerlaw` component is included in this fit. So, `powerlaw` component remains significant as it required to fit high-energy residuals of the atoll sources in the soft state (Pintore et al. 2015; Iaria et al. 2001). This combination of continuum model has been frequently used for the soft state spectra of many atoll type NS LMXBs (Lin et al. 2007; Cackett et al. 2010; Miller et al. 2013). Emission from the boundary layer can also be modelled via low-temperature, optically thick Comptonization. To test this, we replaced the single-temperature blackbody component by the Comptonization model `nthcomp` (Zdziarski et al. 1996; Życki et al. 1999), but the replacement did not improve the fit ($\chi^2/dof=2654/738$). Therefore, we proceeded with the simpler continuum model `tbabs × (diskbb+bbbody+powerlaw)` and use it in all the following analyses.

4.2 Reflection Model

There are two strong emission features around $\sim 5 - 8$ keV and $10 - 20$ keV (see Figure 3), indicating the presence

of a reflection component in the Fe K α region and the corresponding Compton back-scattering hump. In NS systems, the accretion disc may be illuminated by the thermal emission coming from the boundary layer of the NS or by a power-law continuum, resulting in reflected emission. In this observation the continuum of Ser X-1 is dominated by the blackbody component. We therefore included a modified version of the `relionx`¹ model that assumes that the disc is illuminated by a blackbody, rather than a power-law (see e.g. Cackett et al. 2010; King et al. 2016; Degenaar et al. 2016b). The parameters of the `relionx` model include the disc ionization parameter (ξ), the iron abundance (A_{Fe}), the temperature of the ionizing black body flux kT_{refl} and a normalization N_{refl} . In order to account for relativistic Doppler shifts and the gravitational redshifts, we convolved `relionx` with `relconv` (Dauser et al. 2010). Its parameters include the inner and the outer disc emissivity indices (q_{in}, q_{out}), break radius (R_{break}), the inner and outer disk radii R_{in} and R_{out} , the disk inclination (i) and the dimensionless spin parameter (a). In our fits, we used a constant emissivity index (fixed slope) by fixing $q_{out} = q_{in}$ which essentially obviates the meaning of R_{break} .

We imposed a few reasonable conditions when making fits with reflection models. We set the emissivity to $q = 3$, in agreement with a Newtonian geometry far from the NS (Cackett et al. 2010). We set a redshift of $z = 0$ since Ser X-1 is a Galactic source. We fixed the spin parameter $a = 0$ since most NS in LMXBs have $a \leq 0.3$ (Galloway et al. 2008; Miller et al. 2011). The difference of measurement of the position of the R_{ISCO} between $a = 0$ and $a = 0.3$ is less than $1 R_g$ (where $R_g = GM/c^2$). The dimensionless spin parameter a can be approximated as $a \simeq 0.47/P_{ms}$ (Braja et al. 2000) where P_{ms} is the spin period in ms.

¹ https://www-xray.ast.cam.ac.uk/~mlparker/reflionx_models/reflionx_bb.mod

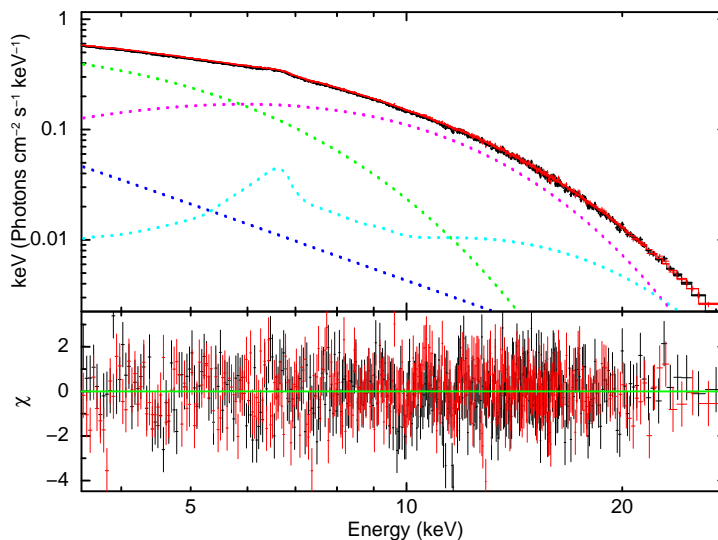


Figure 4. The *NuSTAR* (FPMA in black, FPMB in red) unfolded spectra of Ser X-1 with the best-fitting fitted model consisting of a disk blackbody (green), a single temperature blackbody (purple), a powerlaw (blue) and relativistically blurred reflection (cyan) i.e., $\text{TBabs} \times (\text{diskbb} + \text{body} + \text{powerlaw} + \text{relconv} * \text{reflionx})$. Lower panel shows residuals in units of σ .

The spin period of the source Ser X-1 is unknown as kHz quasi-periodic oscillations (QPOs) and burst oscillations have not been detected so far. We therefore performed the fit with $a = 0$ as well as $a = 0.3$ and found that both the fit yielded similar results. The outer disc radius was fixed to $1000 R_g$.

The addition of the relativistic reflection model improved the spectral fits significantly ($\chi^2/\text{dof} = 885/733$). The best-fitting parameters for the continuum and the reflection spectrum are reported in Table 1. Our fits suggest that the inner disc R_{in} is truncated prior to the ISCO at $(1.7 - 2.3) R_{ISCO}$ ($\simeq 10.2 - 13.8 R_g$ or $23 - 31$ km). The inclination angle is found to be $i \sim 19^\circ$ in agreement with the fact that neither dips nor eclipses have been observed in the light curve of Ser X-1. Additionally, this low inclination angle agrees with the previous *NuSTAR* results (Miller et al. 2013), the *Suzaku* results (Cackett et al. 2010), the *NICER* results (Ludlam et al. 2018) and the results from optical spectroscopy (Cornelisse et al. 2013). The reflection component has an intermediate disc ionization of $\xi \simeq 160 - 232 \text{ erg s}^{-1} \text{ cm}$ which is consistent with $\log \xi \sim (2 - 3)$ seen in other NS LMXBs (Cackett et al. 2010). The iron abundance was found to be $A_{Fe} = 1.5^{+1.6}_{-0.4}$. The fitted spectrum with relativistically blurred reflection model and the residuals are shown in Figure 4.

We computed $\Delta\chi^2$ for the parameters inner disc radius (R_{in}) and the disc inclination angle (i) using **steppar** command in **xspec** to determine how the goodness-of-fit changed as a function of these parameters. The plots of $\Delta\chi^2$ versus i and R_{in} for the best-fit model are shown in the left and right panel of Figure 5, respectively. These plots illustrate the sensitivity of the spectra to the inner extent of the disc as well as to the disc inclination angle. They suggest that the inner disc is truncated prior to the ISCO.

Considering the fact that the reflection parameters are mostly constrained by the iron line, we attempted to fit the data with a relativistic line profile, **relline** model which excludes the broadband features such as the Compton hump seen around $10 - 20$ keV. We measured a line centroid energy of $E = 6.89^{+0.03}_{-0.04}$ keV. The value for the inner disc radius, $R_{in} = 1.76^{+0.15}_{-0.10} R_{ISCO}$ is consistent with our above estimation. We found a small inclination of $i = 12 \pm 3^\circ$ which is also comparable to the previous *NuSTAR* observation. However, the **relline** model, with $\chi^2/\text{dof} = 976/735$, is not as good a fit as the broadband reflection model described above ($\chi^2/\text{dof} = 885/733$). It suggests that the broadband reflection spectrum does make a significant contribution.

Additionally, we tried to fit the spectrum with another flavor of the **reflionx** (Ross & Fabian 2005) model that assumes a high energy exponential cutoff power-law irradiating the accretion disc. To take relativistic blurring into account, we convolved **reflionx** with **relconv** (Dauser et al. 2010). We performed this fit again with the reasonable values of some parameters mentioned above. It did not improved the fit, resulting in a $\chi^2/\text{dof} = 908/733$. This fit led to the smaller blackbody temperature (kT_{bb}) compared to the disc temperature (kT_{disc}) which is quite unphysical. This fit tended towards the larger value of $A_{Fe} \sim 6$. Moreover, disc ionization parameter becomes abnormally high ($\xi \sim 10^4 \text{ erg s}^{-1} \text{ cm}$) and the normalization of the reflection component becomes unfeasibly low ($\sim 2 \times 10^{-6}$). So, we do not comment on it further. The problem may lie in the difference of the shape of the reflection spectrum which assumes an input **powerlaw** to a reflection spectrum that assumes a **blackbody** input spectrum.

5 DISCUSSION

We present here a new *NuSTAR* observation of the bright atoll type NS LMXB Ser X-1. The source displayed a

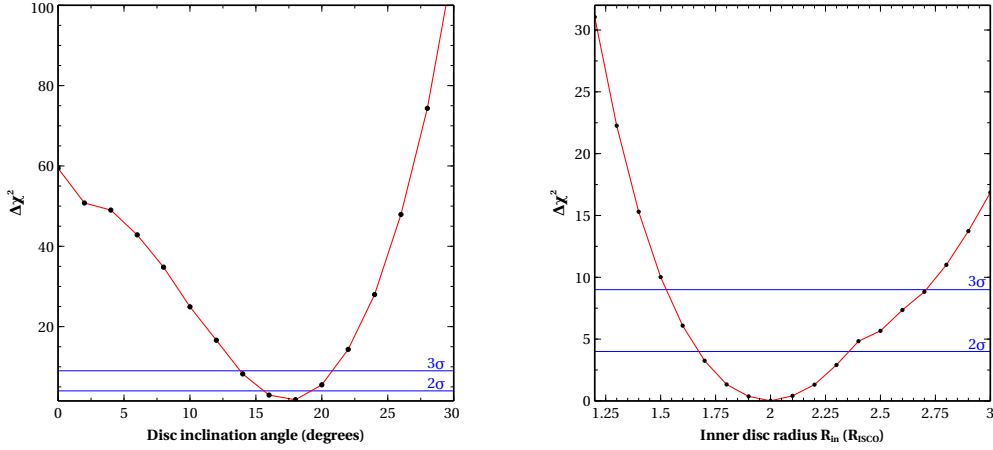


Figure 5. Left panel shows the variation of $\Delta\chi^2 (= \chi^2 - \chi_{min}^2)$ as a function of the disk inclination angle obtained from the relativistic reflection model (`relionx_bb.mod`). We varied the disk inclination angle between 0 degree and 30 degree. Right panel shows the variation of $\Delta\chi^2 (= \chi^2 - \chi_{min}^2)$ as a function of inner disc radius (in the unit of R_{ISCO}) obtained from the relativistic reflection model. We varied the inner disc radius as a free parameter upto $3R_{ISCO}$. The value of the inner disc radius is not consistent with the position of the ISCO. Horizontal lines in both the panels indicate 2σ and 3σ significance level.

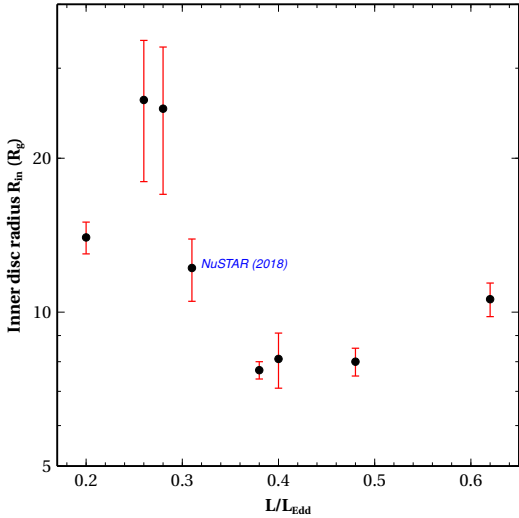


Figure 6. Shows the evolution of the inner disc radius R_{in} (in units of R_g) with the luminosity (based on the data mentioned in Table 2). Inner disc radius does not evolve significantly over the range of $L/L_{Edd} \sim 0.4 - 0.6$ but below this the evolution is significant. A clear trend between R_{in} and L/L_{Edd} is not observed.

particularly soft spectrum with the 3 – 79 keV luminosity of $L_X \sim 0.4 \times 10^{38} \text{ erg s}^{-1}$ which corresponds to $\sim 23\%$ of the Eddington luminosity assuming a distance of 7.7 kpc. The hardness-intensity diagram suggests that the source was in the so-called banana branch during this observation. The broad-band 3 – 30 keV *NuSTAR* energy spectrum can be well described by a continuum model consisting of a disk blackbody (`diskbb`), a single temperature blackbody (`bbbody`) and a power-law (`powerlaw`). Thermal emission from the accretion disc is prominently detected in the X-ray spectrum. The hot blackbody emission provides most of the hard X-ray flux that illuminates the accretion disc and produces the reflection spectrum. In the X-ray spectrum, we clearly detected a broad iron line $\sim 5 - 8$

keV and the Compton back-scattering hump peaking at $\sim 10 - 20$ keV band, indicating the signature of disc reflection phenomenon. These features are best interpreted by a relativistically blurred self-consistent disc reflection model. Studies on reflection spectra provides valuable insight into the accretion geometry, such as the inner radius and the inclination of the accretion disc and the upper limit on the radius of the NS.

From the reflection fit, we found that the inner edge of the accretion disc is truncated prior to the ISCO at $R_{in} = (1.7 - 2.3) R_{ISCO}$, given that $R_{ISCO} = 6 GM/c^2$ for an NS spinning at $a = 0$. This would correspond to $R_{in} = (10.2 - 13.8) R_g$ or (23 – 31) km for a $1.5M_\odot$ NS. The inner disc radius of the source Ser X-1 has been measured by different authors (Ludlam et al. 2018; Chiang et al. 2016b,a; Bhattacharyya & Strohmayer 2007; Matranga et al. 2017; Cackett et al. 2010; Miller et al. 2013) in different flux states using data taken from different satellite missions (see Table 2). The inner disc radius spans a range between $\sim 8 - 25 R_g$ and the flux between $\sim (3 - 11) \times 10^{37} \text{ erg s}^{-1}$ (corresponding to $L/L_{Edd} \sim 0.2 - 0.6$). Therefore, our estimated inner disc radius for Ser X-1 lies within the range obtained from different X-ray missions. It is clear from Figure 6 that comparatively larger values of the inner disc radius are obtained in the lower luminosity states when $L/L_{Edd} \sim 0.2 - 0.35$. At the same time, inner disc radius does not appear to change much when $L/L_{Edd} \sim 0.4 - 0.6$. So, the accretion disc is truncated at larger radius at fluxes $< 0.4L/L_{Edd}$ (see also Chiang et al. 2016b). The larger inner radii are mainly obtained from the *XMM-Newton* observations which are less reliable in comparison to other archival data due to short exposure and calibration issues of EPIC-PN timing mode data (Walton et al. 2012). From the previous *NuSTAR* observation, Miller et al. (2013) found the inner disc radius to be $10.6 \pm 0.6 R_g$ when the luminosity of the source was $L_X \sim 1.1 \times 10^{38} \text{ erg s}^{-1}$ ($\sim 62\%$ of the Eddington luminosity) based on 0.5 – 40 keV flux and assuming a distance of 7.7 kpc. From

Table 1. Best-fitting spectral parameters of the *NuSTAR* observation of the source *Ser X-1* using model: `TBabs×(diskbb+body+powerlaw+relconv*reflionx)`.

Component	Parameter (unit)	Value
TBABS	$N_H (\times 10^{21} \text{ cm}^{-2})$	4.0(<i>f</i>)
DISKBB	$kT_{disc} (\text{keV})$	$1.43^{+0.28}_{-0.19}$
	norm $[(\text{km}/10 \text{ kpc})^2 \cos i]$	50^{+42}_{-28}
BBODY	$kT_{bb} (\text{keV})$	2.09 ± 0.14
	norm $(\times 10^{-2})$	$3.08^{+0.26}_{-0.49}$
POWERLAW	Γ	3.32 ± 0.23
	norm	$0.88^{+0.84}_{-0.85}$
RELCONV	i (degrees)	19^{+2}_{-1}
	$R_{in} (\times R_{ISCO})$	2.0 ± 0.3
REFLIONX	$\xi (\text{erg cm s}^{-1})$	193^{+39}_{-33}
	$kT_{refl} (\text{keV})$	$2.95^{+0.12}_{-0.18}$
	$A_{Fe} (\times \text{solar})$	$1.44^{+1.56}_{-0.34}$
	norm	$1.41^{+0.50}_{-0.61}$
	$F_{total}^* (\times 10^{-9} \text{ ergs/s/cm}^2)$	5.0 ± 0.01
	$F_{diskbb} (\times 10^{-9} \text{ ergs/s/cm}^2)$	2.0 ± 0.01
	$F_{bbody} (\times 10^{-9} \text{ ergs/s/cm}^2)$	2.4 ± 0.01
	$F_{powerlaw} (\times 10^{-9} \text{ ergs/s/cm}^2)$	0.25 ± 0.01
	$F_{reflionx} (\times 10^{-9} \text{ ergs/s/cm}^2)$	0.40 ± 0.01
	$L_{3-30\text{keV}} (\times 10^{38} \text{ ergs/s})$	0.4 ± 0.01
	χ^2/dof	885/733

The outer radius of the `relconv` spectral component was fixed to $1000 R_g$. The dimensionless spin parameter (a) and redshift (z) were set to zero. We fixed emissivity index $q = 3$, assumed a distance of 7.7 kpc and a mass of $1.5 M_\odot$ for calculating the luminosity. *All the unabsorbed fluxes are calculated in the energy band 3.0 – 79.0 keV.

this observation, we found an inner disc radius $12.2 \pm 1.7 R_g$ when the source luminosity was $L_X \sim 0.54 \times 10^{38} \text{ erg s}^{-1}$ ($\sim 31\%$ of the Eddington luminosity) based on 0.5 – 40 keV flux and assuming the same distance of 7.7 kpc. Therefore, it seems that the disc appears to move outward slightly during the low luminosity state. Thus, comparing with the previous *NuSTAR* observation, we can re-established the commonly assumed fact that the accretion disc in LMXBs moves away from the NS when the X-ray luminosity decays (Ludlam et al. 2017). However, it may be noted that Matranga et al. (2017) have re-analyzed the same *NuSTAR*

Table 2. Luminosity and inner disc radius (R_{in}) of previous *Ser X-1* observations.

Observation	L/L_{Edd}	Radius R_{in} (R_g)
<i>XMM</i> ¹ (2004, Obs ID 0084020401)	0.28	25 ± 8
<i>XMM</i> ¹ (2004, Obs ID 0084020501)	0.20	14 ± 1
<i>XMM</i> ¹ (2004, Obs ID 0084020601)	0.26	26 ± 8
<i>Suzaku</i> ¹ (2006)	0.48	8 ± 0.3
<i>NuSTAR</i> ² (2013)	0.62	10.6 ± 0.6
<i>Chandra</i> ³ (2014)	0.38	7.7 ± 0.1
<i>Suzaku</i> ⁴ (2014)	0.40	8.1 ± 0.8
<i>NuSTAR</i> ⁵ (2018)	0.31	12.2 ± 1.7

Information collected from ¹Cackett et al. (2010), ²Miller et al. (2013), ³Chiang et al. (2016a), ⁴Chiang et al. (2016b), ⁵present work. The luminosity was calculated based on the 0.5 – 25 keV absorption-corrected flux and a distance of 7.7 kpc. For more details see Table 4 of Chiang et al. (2016b).

observation as done by Miller et al. (2013) with a slightly different continuum and reflection models and found the inner disc radius to be $\sim 13 R_g$.

The ISCO of a gravitating source depends on the mass and radius of the NS. The value of ISCO lie somewhere between 5 – 6 R_g for some reasonable parameters. Our measured inner disc radius of $\sim 12 R_g$ is therefore larger than the expected ISCO and the NS surface. The disc could therefore be truncated by either the boundary layer which lies between the disc and the NS surface or by the associated NS magnetic field. From the persistent flux (F_p) and the distance (d) of the source, we estimate the mass accretion rate (\dot{m}) per unit area at the NS surface (Galloway et al. 2008). Here we used Equation (2) of Galloway et al. (2008)

$$\dot{m} = 6.7 \times 10^3 \left(\frac{F_p c_{bol}}{10^{-9} \text{ erg cm}^{-2} \text{ s}^{-1}} \right) \left(\frac{d}{10 \text{ kpc}} \right)^2 \left(\frac{M_{NS}}{1.4 M_\odot} \right)^{-1} \times \left(\frac{1+z}{1.31} \right) \left(\frac{R_{NS}}{10 \text{ km}} \right)^{-1} \text{ g cm}^{-2} \text{ s}^{-1}, \quad (1)$$

where c_{bol} is the bolometric correction which is ~ 1.38 for the nonpulsing sources (Galloway et al. 2008). M_{NS} and R_{NS} are the mass and radius of the NS, respectively. z is the surface redshift and $1+z = 1.31$ for a NS with mass $1.4 M_\odot$ and radius 10 km. We determine the mass accretion rate using $F_p = 5.0 \times 10^{-9} \text{ erg s}^{-1} \text{ cm}^2$ to be $\sim 5.4 \times 10^{-9} M_\odot \text{ y}^{-1}$ during this observation. It is consistent when the atoll sources lie in the banana branch. From the inferred mass accretion rate, we estimate the maximum radial extent (R_{max}) of the boundary layer region using Equation (2) of

Popham & Sunyaev (2001)

$$\log(R_{\max} - R_{\text{NS}}) \simeq 5.02 + 0.245 \left| \log \left(\frac{\dot{m}}{10^{-9.85} M_{\odot} \text{ yr}^{-1}} \right) \right|^2 \quad (2)$$

It gives a maximum radial extent of $\sim 6.4 R_g$ for the boundary layer (assuming $M_{\text{NS}} = 1.5 M_{\odot}$ and $R_{\text{NS}} = 10$ km). This is consistent with the location of the inner disc radius measured from spectral modelling.

The inferred boundary layer is smaller than the disc truncation radius. So, it is more likely that the magnetic field is responsible for the disc truncation in this source. If the disc is truncated by the magnetosphere, we can estimate an upper limit on the strength of the magnetic field of the NS using the upper limit of $R_{\text{in}} = 13.9 R_g$ measured from the reflection fit. We used Equation (1) of Cackett et al. (2009) to calculate the magnetic dipole moment (μ). Assuming a mass of $1.5 M_{\odot}$, taking the distance to be 7.7 kpc and using the unabsorbed flux from 0.01 – 100 keV of $8.5 \times 10^{-9} \text{ erg cm}^{-2} \text{ s}^{-1}$ as the bolometric flux (F_{bol}), we determine $\mu \sim 8.2 \times 10^{26} \text{ G cm}^3$ (assuming $k_A = 1$, $f_{\text{ang}} = 1$ and $\eta = 0.1$). This corresponds to a magnetic field strength of $B \leq 1.6 \times 10^9 \text{ G}$ at the magnetic poles for a NS of radius 10 km. This order of magnetic field has the potential to truncate an accretion disc far from the stellar surface (Mukherjee et al. 2015).

Another possibility of disc truncation may be due to the state transition associated with a receding disc which is related with a low luminosity and hard power-law dominated X-ray spectra (Esin et al. 1997). The Ser X-1 spectra presented here are taken in a soft, high luminosity state. Moreover, no state transition has been observed from the HR or HID. Significant disc truncation only occurs at a high enough magnetic field and low mass accretion rate, although there are examples where disc truncation occurs at higher luminosities too (King et al. 2016). Therefore, a significant disc truncation scenario can only be tested if the source Ser X-1 is observed in a low luminosity and hard spectral state. So, the evolution of the inner disc radius remains unclear as the source has only been observed in the high luminosity and soft spectral state.

6 ACKNOWLEDGEMENTS

This research has made use of data and/or software provided by the High Energy Astrophysics Science Archive Research Centre (HEASARC). This research also has made use of the *NuSTAR* data analysis software (**NuSTARDAS**) jointly developed by the ASI science center (ASDC, Italy) and the California Institute of Technology (Caltech, USA). ASM would like to thank Inter-University Centre for Astronomy and Astrophysics (IUCAA) for hosting him during subsequent visits. BR also likes to thank IUCAA for their hospitality and facilities extended to him under their Visiting Associate Programme.

REFERENCES

- Makishima K., Takeshima T., Kawabata K., 1993, PASJ, 45, 801
- Ballantyne D. R., Ross R. R., Fabian A. C., 2001, MNRAS, 327, 10
- Bhattacharyya S., 2011, MNRAS, 415, 3247
- Bhattacharyya S., Strohmayer T. E., 2007, ApJ, 664, L103
- Bowyer S., Byram E. T., Chubb T. A., Friedman H., 1965, Science, 147, 394
- Braje T. M., Romani R. W., Rauch K. P., 2000, ApJ, 531, 447
- Cackett E. M., Altamirano D., Patruno A., Miller J. M., Reynolds M., Linares M., Wijnands R., 2009, ApJ, 694, L21
- Cackett E. M. et al., 2010, ApJ, 720, 205
- Cackett E. M. et al., 2008, ApJ, 674, 415
- Chiang C.-Y. et al., 2016a, ApJ, 821, 105
- Chiang C.-Y., Morgan R. A., Cackett E. M., Miller J. M., Bhattacharyya S., Strohmayer T. E., 2016b, ApJ, 831, 45
- Church M. J., Balucińska-Church M., 2001, A&A, 369, 915
- Cornelisse R., Casares J., Charles P. A., Steeghs D., 2013, MNRAS, 432, 1361
- Cornelisse R., Kuulkers E., in't Zand J. J. M., Verbunt F., Heise J., 2002, A&A, 382, 174
- Dauser T., Wilms J., Reynolds C. S., Brenneman L. W., 2010, MNRAS, 409, 1534
- Degenaar N. et al., 2016a, MNRAS, 461, 4049
- Degenaar N., Koljonen K. I. I., Chakrabarty D., Kara E., Altamirano D., Miller J. M., Fabian A. C., 2016b, MNRAS, 456, 4256
- Degenaar N., Miller J. M., Chakrabarty D., Harrison F. A., Kara E., Fabian A. C., 2015, MNRAS, 451, L85
- Dickey J. M., Lockman F. J., 1990, ARAA, 28, 215
- Esin A. A., McClintock J. E., Narayan R., 1997, ApJ, 489, 865
- Fabian A. C., Iwasawa K., Reynolds C. S., Young A. J., 2000, PASP, 112, 1145
- Galloway D. K., Muno M. P., Hartman J. M., Psaltis D., Chakrabarty D., 2008, ApJS, 179, 360
- Hasinger G., van der Klis M., 1989, A&A, 225, 79
- Homan J. et al., 2010, ApJ, 719, 201
- Iaria R., Di Salvo T., Burderi L., Robba N. R., 2001, ApJ, 548, 883
- King A. L. et al., 2016, ApJ, 819, L29
- Li F. K., Lewin W. H. G., Clark G. W., Doty J., Hoffman J. A., Rappaport S. A., 1977, MNRAS, 179, 21P
- Lin D., Remillard R. A., Homan J., 2007, ApJ, 667, 1073
- Ludlam R. M. et al., 2018, ApJ, 858, L5
- Ludlam R. M. et al., 2019, ApJ, 873, 99
- Ludlam R. M., Miller J. M., Degenaar N., Sanna A., Cackett E. M., Altamirano D., King A. L., 2017, ApJ, 847, 135
- Matranga M., Di Salvo T., Iaria R., Gambino A. F., Burderi L., Riggio A., Sanna A., 2017, A&A, 600, A24
- Miller J. M., Maitra D., Cackett E. M., Bhattacharyya S., Strohmayer T. E., 2011, ApJ, 731, L7
- Miller J. M. et al., 2013, ApJ, 779, L2
- Mukherjee D., Bult P., van der Klis M., Bhattacharya D., 2015, MNRAS, 452, 3994
- Oosterbroek T., Barret D., Guainazzi M., Ford E. C., 2001, A&A, 366, 138
- Pandel D., Kaaret P., Corbel S., 2008, ApJ, 688, 1288
- Pintore F. et al., 2015, MNRAS, 450, 2016

- Piraino S., Santangelo A., Kaaret P., 2000, A&A, 360, L35
- Popham R., Sunyaev R., 2001, ApJ, 547, 355
- Reis R. C., Fabian A. C., Young A. J., 2009, MNRAS, 399, L1
- Remillard R. A., Lin D., ASM Team at MIT, NASA/GSFC, 2006, The Astronomer's Telegram, 696, 1
- Ross R. R., Fabian A. C., 2005, MNRAS, 358, 211
- Ross R. R., Fabian A. C., 2007, MNRAS, 381, 1697
- Shakura N. I., Sunyaev R. A., 1973, A&A, 500, 33
- Swank J. H., Becker R. H., Pravdo S. H., Serlemitsos P. J., 1976, IAUC, 2963, 1
- Verner D. A., Ferland G. J., Korista K. T., Yakovlev D. G., 1996, ApJ, 465, 487
- Walton D. J., Reis R. C., Cackett E. M., Fabian A. C., Miller J. M., 2012, MNRAS, 422, 2510
- Wilms J., Allen A., McCray R., 2000, ApJ, 542, 914
- Zdziarski A. A., Johnson W. N., Magdziarz P., 1996, MNRAS, 283, 193
- Życki P. T., Done C., Smith D. A., 1999, MNRAS, 309, 561